ORIGINAL PAPER

Experimental and Theoretical Study on Frost Deformation and Damage of Red Sandstones with Different Water Contents

Shibing Huang[1,2] · Yuantian Cai[1] · Yanzhang Liu[1,2] · Guofeng Liu[3]

Abstract

Volumetric expansion of water by 9% in saturated pores and cracks causes substantial frost deformation in rock masses. Frost deformation is an important index reflecting the frost resistance of rocks; however, water saturation has a great influence on the frost deformation characteristics. In this research, the frost strains and acoustic emission activities of red sandstone with different water saturations are monitored under freeze–thaw conditions. The experimental results show that both the peak and the residual frost heaving strains greatly increase for sandstone beyond 85% water saturation. However, there is no significant frost heaving strain that occurs in low-saturation red sandstone (less than 85% water saturation). The acoustic emission activities show the same change trend and further confirm the existence of this critical saturation. In addition, the pore size distribution also has a great influence on the frost heaving strain and freeze–thaw damage. All the liquid pore water in this red sandstone is frozen at − 20 °C because the pores are larger than the critical freezing radius (2.58 nm at − 20 °C) according to the measured pore size distribution. Based on the pore micromechanics and Gibbs–Thomson equation, a developed frost heaving model is proposed considering the effects of water saturation and the pore size distribution. The proposed model can be used to predict the frost heaving strain at any freezing temperature for unsaturated red sandstone. This study thus provides the frost deformation characteristics of red sandstone and contributes to a better understanding of the freeze–thaw damage mechanism of unsaturated sandstone.

Keywords Frost deformation · Acoustic emission · Water saturation · Unsaturated sandstone · Frost damage

✉ Shibing Huang
huangshibing@wust.edu.cn; huangshibing@wust.edu.cn

✉ Yanzhang Liu
liuyanzhang@163.com; liuyanzhang@163.com

Yuantian Cai
wkdcyt@163.com

Guofeng Liu
gfliu@chd.edu.cn

[1] School of Resources and Environmental Engineering, Wuhan University of Science and Technology, Wuhan, China

[2] Hubei Key Laboratory for Efficient Utilization and Agglomeration of Metallurgic Mineral Resources, Wuhan, China

[3] Key Laboratory for Bridge and Tunnel of Shaanxi Province, School of Highway, Chang'an University, Xi'an, Shaanxi, China

List of Symbols

ρ_r, ρ_i, ρ_l	Densities of rock matrix, solid ice and water, respectively
UCS	Uniaxial compressive strength
E_r, E_i	Elastic moduli of red sandstone and solid ice, respectively
μ_r, μ_i	Poisson's ratio of red sandstone and solid ice, respectively
n	Porosity of red sandstone
v_r	P-wave velocity of rock
α_r	Thermal expansion coefficient of rock
ℓ	Latent heat per unit mass of water
T_m	Freezing point of bulk water
γ_{il}	Free energy of ice-liquid interfacial
m_{r1}, m_{r2}	Masses of the red sandstone sample before and after sticking the strain gauges
m_d, m_{s1}	Masses of the dry and saturated red sandstone sample, respectively
m_t	Mass of the sandstone sample corresponding to the specific saturation
S_r	Saturation of rock

ε_n^d, ε_r^d	Total nominal strain and the actual strain of dry red sandstone, respectively
ε_e	Strain error
T, T_0	Current temperature and initial temperature, respectively
α_n^d	Nominal thermal expansion coefficient of red sandstone
α_r^d	Actual thermal expansion coefficient of red sandstone
α_e	Thermal expansion coefficient of the glue and strain gauge
ε_p^{sa}	Peak frost heaving strain of saturated sandstone
ε_{re}^{sa}	Residual strain of saturated sandstone
a_1, b_1, a_2, b_2	Unknown frost heaving parameters
K_r	Bulk modulus of rock
ε_T	Linear thermal strain
ε_f	Linear frost heaving strain caused by ice pressure
b	Biot coefficient
p_i^s	Equivalent pore ice pressure
$w_u(T)$	Unfrozen water content
$F(r)$	Cumulative distribution function of the pore size
r	Radius of the sphere pore
m_1, m_2	Characteristic size of coarse pores and thin pores, respectively
V_1, V_2	Volume fractions of the coarse and thin pores, respectively.
$\xi(S_r)$	Impact coefficient of water saturation

1 Introduction

The breakdown of rocks and cement-based materials under freeze–thaw cycles is an important subject with broad repercussions in geotechnical engineering and building materials (Tan et al. 2014; Freire-Lista et al. 2015; Xia et al. 2018; Hu et al. 2018; Eslami et al. 2018; Zhou et al. 2019). Under a low temperature, a considerable frost heaving pressure will be produced in pores due to water freezing. This pressure is mainly responsible for the freeze–thaw damage of porous rocks (Hori and Morihiro 1998; Tan et al. 2018; Liu et al. 2019; Jia et al. 2020a, b; Huang et al. 2018b). The degree of freeze–thaw damage in rocks has been widely investigated, and many prediction models have been proposed in previous studies (Liu et al. 2015; Wang et al. 2016; Huang et al. 2018a; Fu et al. 2018; Fang et al. 2019; Lu et al. 2019). The damage indexes in these models are expressed by the mechanical strength, porosity and P-wave (primary wave) velocity (Luo et al. 2014; Park et al. 2015; Momeni et al. 2016; Sarici and

Ozdemir 2018; Wang et al. 2019; Fang et al. 2019; Zhang et al. 2021). However, these indexes are difficult to test in the laboratory. For instance, the strength tests of rocks under freeze–thaw cycles are extremely laborious and time-consuming (Liu et al. 2015). In addition, the P-wave velocity and porosity are hard to continuously monitor in the laboratory because the rock samples must be removed from the freeze box when the P-wave velocity or porosity is measured. Fortunately, frost deformation is a readily available physical parameter, that can be continuously monitored by strain gauges under freeze–thaw cycles (Lv et al. 2019). The frost heaving strain can reflect the freezing process of pore water and the damage degree after freeze–thaw cycles. A larger irreversible residual frost heaving strain implies more serious freeze–thaw damage (Zhao et al. 2015; Wang et al. 2020; Huang et al. 2020b). Therefore, studying the frost deformation characteristics of porous rocks under freeze–thaw cycles is significant.

The theoretical value of frost deformation was first studied by Mellor (1970) without considering the confining pressure of the pore wall. Then, Matsuoka (1990) measured the linear strains of different saturated rocks under freezing using foil strain gauges. The test results showed that water migration has an influence on the freezing expansion of rocks when in contact with water in an open system. Yamabe and Neaupane (2001) also used this method to monitor the linear strains of Sirahama sandstone and proposed that the induced strains for wet samples were significantly larger than those of dry samples. Jia et al. (2015) measured the frost deformation of red sandstone with saturations of 50% and 90% using strain gauges. Similarly, the irreversible residual frost heaving strains only occurred in the samples with 90% water saturation. Recently, Lv et al. (2019) used the strain gauges to investigate the difference in frost heaving strains under uniform and unidirectional freezing conditions. Therefore, strain tests under low temperatures can reveal the frost heaving process of rocks and the main influencing factors, including the freezing temperature, porosity, rock properties and water conditions.

Furthermore, water saturation has been shown to be a remarkable influencing factor on the freeze–thaw damage degree of rocks (Prick et al. 1997). Chen et al. (2004) found that the P-wave velocity decreased quickly and that porosity increased if the initial degree of saturation was beyond 60%. Binal (2009) proposed that 75% saturation could cause a change in the physical and mechanical properties of rock samples under freeze–thaw cycles. Al-Omari et al. (2015) claimed that the porosity of limestones quickly increased when the degree of saturation exceeded 85%. Therefore, there should be a critical saturation for rocks to cause serious damage under freeze–thaw cycles. Therefore, in this study, the influence of the water saturation on the freeze–thaw damage of red sandstone is investigated from a new perspective

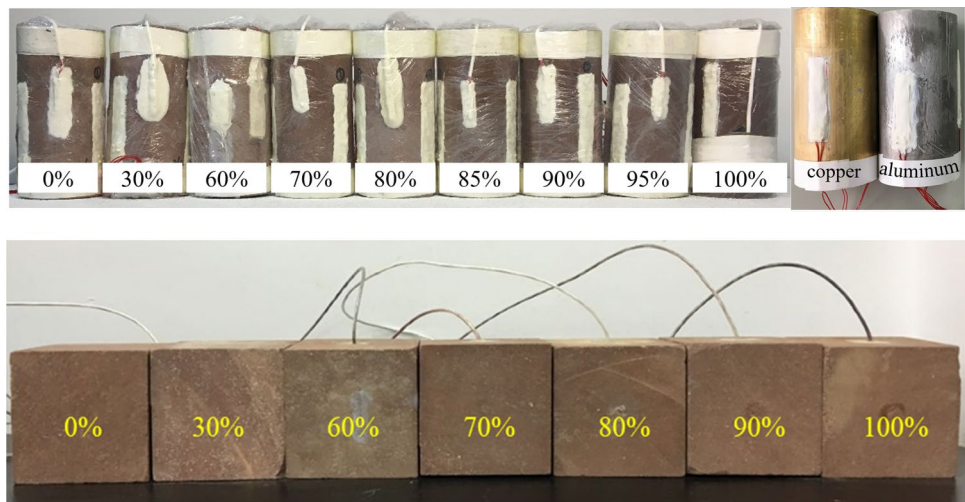**Fig. 1** The red sandstone, copper and aluminum samples

Table 1 The basic physico-mechanical properties of the red sandstone

ρ_r (kg/m³)	UCS (MPa)	E_r (Gpa)	μ_r	n (%)	v_r (km/s)	α_r (°C⁻¹)
2400	52.7	9.54	0.25	11.9	2.46	9.4×10^{-6}

of frost deformation combined with AE (acoustic emission) technology.

2 Materials and Methods

2.1 Basic Properties of the Red Sandstone

The red sandstone samples were collected from Yichang, Hubei Province. This dark red sandstone is a typical calcareous cemented medium quartz sandstone with an obvious coarse sand structure. It is widely distributed throughout the reservoir bank slope. According to the suggested ISRM method, nine homogenous sandstone samples with a diameter of 50 mm and a height of 100 mm and seven $100 \times 100 \times 100$ mm³ cubic sandstone samples were prepared (Fig. 1). The basic physico-mechanical properties of these red sandstones are listed in Table 1. The mineral components of this red sandstone were measured by XRD (X-ray diffraction), and are composed of feldspar (43.25%), quartz (36.07%), calcite (9.44%), illite (7.24%) and chlorite (4%), as shown in Fig. 2.

The pore structure has a significant influence on the freezing process of the pore water. Therefore, the pore size distribution of this red sandstone was measured using MIP (mercury intrusion porosimetry) accompanied by gas adsorption by the BET (BET is short for three famous scientists, Brunauer, Emmett and Tellor) method. The MIP method is used to measure pore sizes larger than 40 nm, and the BET method is used to measure pore sizes smaller than 55 nm. The pore size distribution derived by these two test
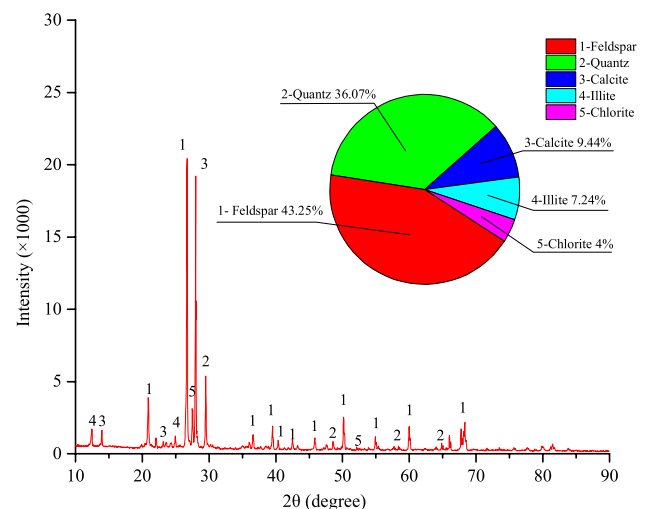

Fig. 2 X-ray diffraction pattern of the red sandstone (Huang et al. 2020b)

methods is plotted in Fig. 3. It shows that micropores (< 15 μm) occupy most of the pore volume.

2.2 Experimental Procedure

There were nine standard cylinder sandstone samples with water saturation degrees of 0%, 30%, 60%, 70%, 80%, 85%, 90%, 95% and 100%, respectively. These nine standard cylindrical samples were used to measure the linear strains with the temperature during the freeze–thaw process. The linear strains were continuously monitored by strain gauges
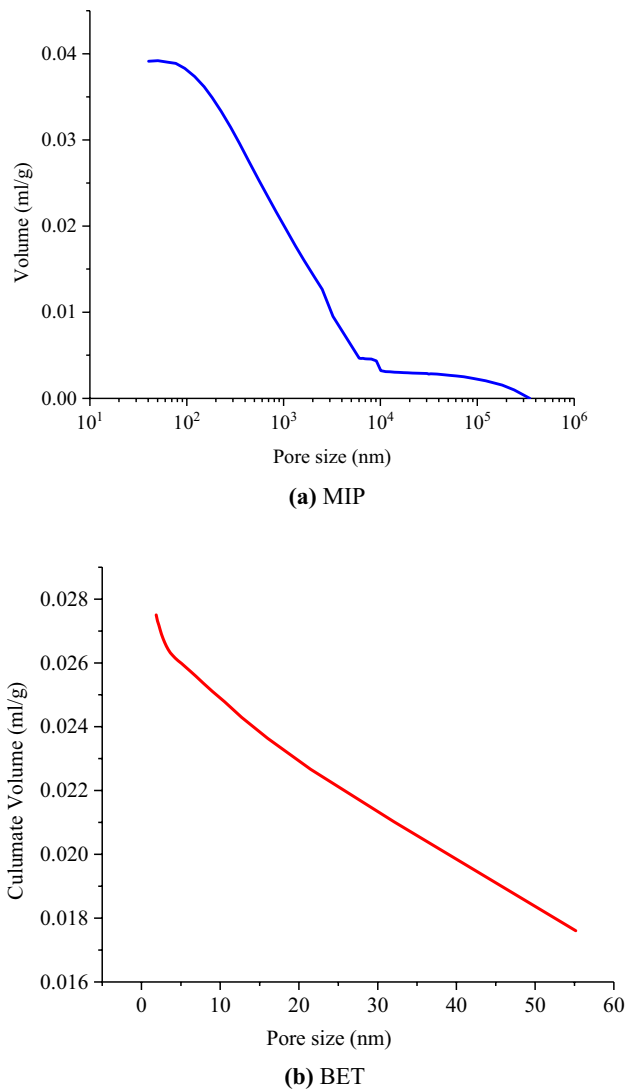
(a) MIP

(b) BET

Fig. 3 Cumulative pore size distribution of the red sandstone

and a strain collection device, and the temperature variations of these cylindrical sandstone samples were monitored by the PT-100 temperature sensor. For these cylindrical samples, the PT-100 sensors were attached to the surface of these samples and covered with a heat insulation adhesive. During the freeze–thaw process, the rock samples were first put into the freeze box at − 20 °C to freeze for 6 h. They were then gradually thawed in an air-conditioned room at a temperature of approximately 20 °C and a humidity of 56% for 6 h. This time is long enough for the complete freezing and thawing of the whole sample by measuring the internal temperature. Therefore, the time of one freeze–thaw cycle was approximately 12 h for the standard cylindrical sandstone samples.

In addition, to avoid mutual adverse interference, seven $100 \times 100 \times 100$ mm^3 cubic sandstone samples were prepared to track the AE activities of the sandstone during one

freeze–thaw cycle. These seven cubic sandstone samples contain water saturations of 0%, 30%, 60%, 70%, 80%, 90% and 100%. The internal temperature of these cubic sandstone samples was monitored by a PT-100 temperature sensor. The PT 100 sensors were embedded inside these cubic samples by drilling a small hole. An 8-channel AE instrument (DS2) and eight high sensitivity sensors (RS-2A) were used to monitor the AE activities of the sandstone during the freeze–thaw process. The frequency response range of these sensors is 20–400 kHz. The preamplifier of the AE system was set as 40 dB and the sampling frequency was 3 MHz. The intermittent continuous mode was adopted to monitor the AE signals in sandstone for 24 h during one freeze–thaw cycle. The main experimental devices are shown in Fig. 4.

An important preparation procedure is to accurately determine the different water saturations for these sandstone samples. This procedure can be summarized as follows: (1) the samples were placed in an electric drying oven with forced convection at 110 °C for 48 h until the mass remained constant. Then, the masses of dry samples were measured after cooling, denoted by m_d. (2) The dry samples were placed into a vacuum device at − 0.1 MPa to extract air for 6 h. Afterwards, water was injected into this vacuum device to submerge the rock samples in water for 24 h. Then, the completely saturated samples were extracted, and their mass was recorded as m_{s1}. (3) All the saturated sandstone samples were placed in an air-conditioned room (temperature of 20 ± 2 °C, humidity of 56%) to gradually dehydrate until natural conditions were reached. (4) Then, strain gauges were placed at the designed positions on the red sandstone samples. The masses of the samples were recorded as m_{r1} and m_{r2} before and after attaching the strain gauges, respectively. Therefore, the total mass of the 704 glue (704 silicone rubber sealant glue), the special adhesive glue (a kind of superbonder glue) and the strain gauges on the surface of the sample was $\Delta m_g = m_{r1} − m_{r2}$. (5) The samples with attached strain gauges were forced to be completely saturated by repeating step 2. (6) All the saturated sandstone samples were placed in the air-conditioned room again to gradually dehydrate until the specified mass m_t was reached. The natural dehydration process was continuously monitored by a high-accuracy electronic balance with a precision of 0.01 g until the predetermined mass was reached. Then, the sample was immediately wrapped with plastic film to prevent water loss. More details about the procedure of preparing samples with different saturations can be found in our previous literature (Liu et al. 2020; Huang et al. 2021).

The mass of the sample corresponding to the specified water saturation can be expressed as:

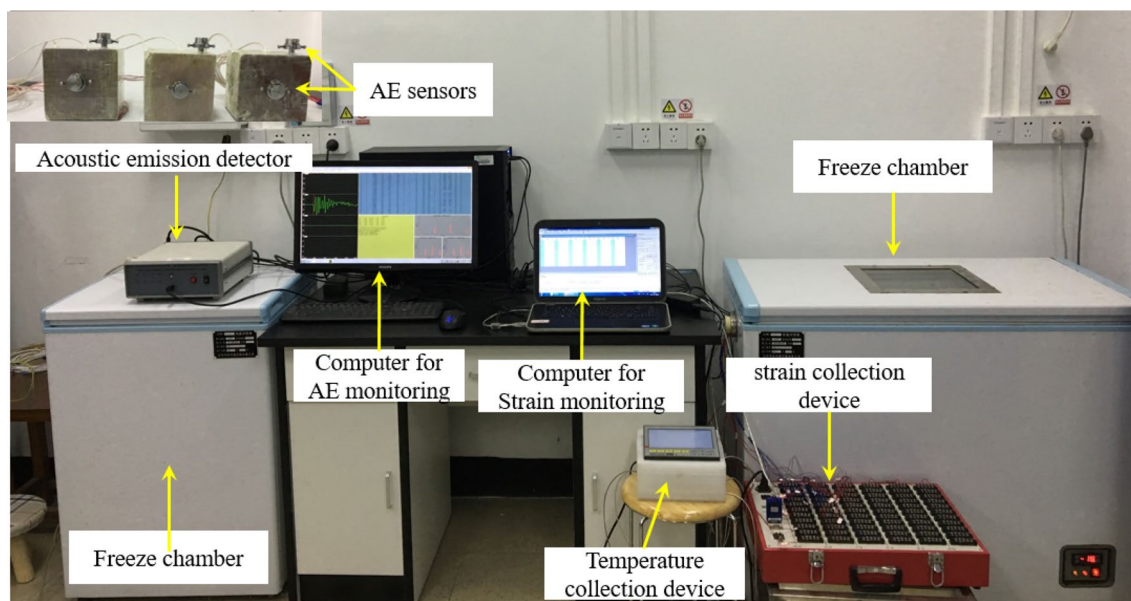$$m_t = S_r(m_{s1} − m_d) + m_d + \Delta m_g, \tag{1}$$
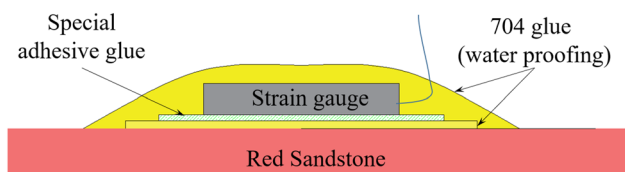
Fig. 4 The main experimental devices

Fig. 5 The structure of attached strain gauges

where m_t is the specified mass corresponding to the set saturation S_r, $\Delta m_g = m_{r1} - m_{r2}$ is the total mass of the 704 glue, the special adhesive glue and the strain gauges on the surface of the sample, and m_{s1} and m_d are the masses of the saturated and dry red sandstone, respectively.

This procedure for measuring the freeze–thaw deformation of rocks by strain gauges is advantageously simple and inexpensive. To ensure that the strain gauges and wet red sandstone samples were closely bonded and to prevent the strain gauges from contacting the internal moisture of the sandstone, a thin waterproof layer of 704 glue was first attached onto the surface of the sandstone, followed by special adhesive glue and strain gauges. Then, an external waterproof layer of 704 glue was attached to the strain gauges again to prevent external moisture from interfering (Fig. 5). However, the temperature effect on the strain gauge sensitive grid and glue will cause experimental error at low temperatures. Therefore, a novel compensation method was adopted to correct the measured strain at low temperatures.

The strain of the dry red sandstone with a known coefficient of thermal expansion was measured by quarter bridge compensation. The actual strain of red sandstone can be expressed as

$$\varepsilon_r^d = \varepsilon_n^d - \varepsilon_e, \tag{2}$$

where ε_n^d and ε_r^d are the total nominal strain and the actual strain of the dry red sandstone, respectively, and ε_e is the error strain caused by the temperature effect on the 704 glue and strain gauge.

It should be noted that the copper and aluminum standard samples used in this study are only used to verify the reliability of the experimental results of the frost heaving strain. In addition, completely dry red sandstone is used as a compensation block to eliminate the low-temperature effect on the glue and strain gauge deformation.

2.3 Validation of the Test Method

The total nominal strain of dry sandstone decreases linearly with decreasing temperature (Fig. 6). Therefore, we can obtain

$$\varepsilon_n^d = \alpha_n^d(T - T_0), \tag{3}$$

where T and T_0 are the present freezing temperature and the initial temperature, respectively, and α_n^d is the nominal thermal expansion coefficient of the red sandstone.

Similarly, the actual thermal strain of dry red sandstone is
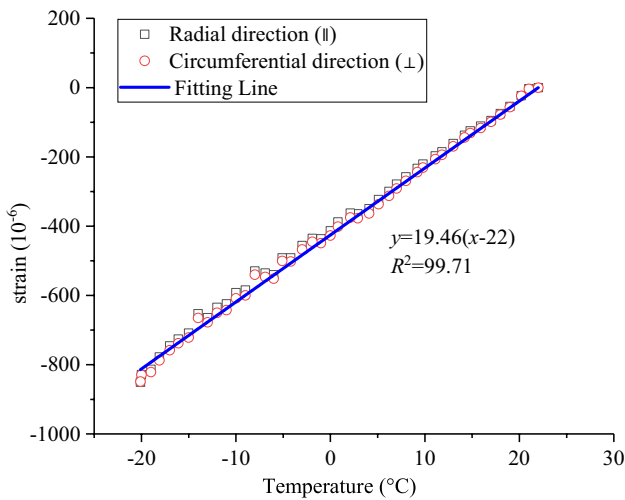
$$\varepsilon_r^d = \alpha_r^d(T - T_0), \tag{4}$$

Fig. 6 The nominal strains of the dry sandstone

(a) The original strains before correction

where α_r^d is the actual thermal expansion coefficient of the red sandstone.

Substituting Eqs. (3) and (4) into Eq. (2) yields

$$\varepsilon_e = (\alpha_n^d - \alpha_r^d)(T - T_0). \tag{5}$$

Therefore, the total thermal expansion coefficient of the glue and strain gauge can be written as
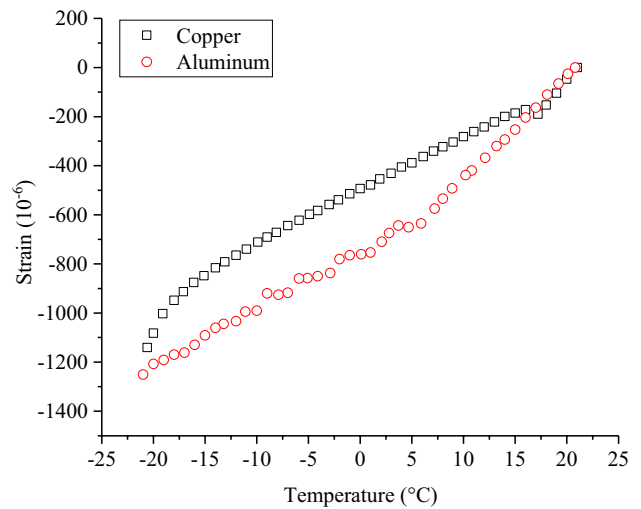
$$\alpha_e = \alpha_n^d - \alpha_r^d. \tag{6}$$

By fitting the measured nominal thermal strain of the red sandstone (Fig. 6), the nominal thermal expansion coefficient of red sandstone is $\alpha_n^d = 19.46 \times 10^{-6}/°C$. Substituting the actual thermal expansion coefficient of dry red sandstone $\alpha_r^d = 9.4 \times 10^{-6}/°C$ into Eq. (6), yields
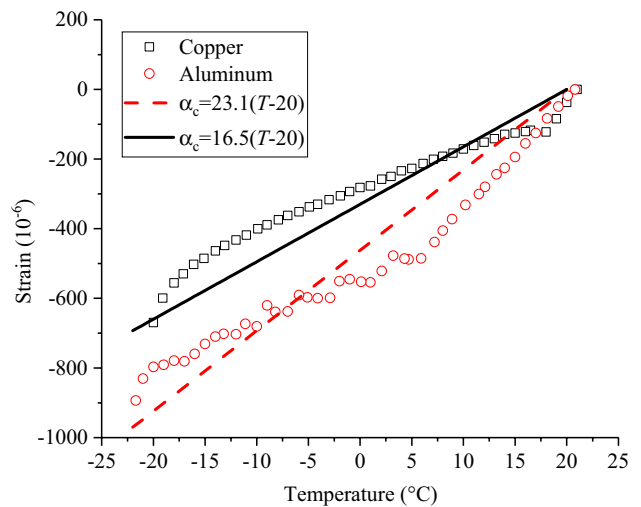
$$\alpha_e = 10.06 \times 10^{-6}/°C. \tag{7}$$

Equation (7) is used to correct the thermal strain of red sandstone with different water saturations to eliminate the influence of the glue and strain gauge on the frost heaving strains of the red sandstone samples.

The linear strains of the copper and aluminum standard samples during one freeze–thaw cycle are shown in Fig. 7. Equation (7) is used to correct the strains of the copper and aluminum standard samples during one freeze–thaw cycle, by eliminating the strain error caused by the thermal effect of the glue and strain gauge. The measured values of the thermal expansion coefficient for the copper and aluminum standard samples are compared with the theoretical values in Table 2. This shows that the theoretical values are very close to the corrected experimental values. Therefore, the strain correction method introduced before is reliable.

(b) The actual strains after correction

Fig. 7 The original and corrected thermal strains of copper and aluminum under freezing

Table 2 The thermal expansion coefficient of the the copper and aluminum

Material	Thermal expansion coefficient/(10^{-6} °C^{-1})	
	Experiment	Reference (Lide 2004)
Copper	16.3	16.5
Aluminum	21.02	23.1

3 Experimental Results

3.1 The Influence of Water Saturation on the Temperature of Red Sandstone

The internal temperature variations of these red sandstone samples against the freeze–thaw time are plotted in Fig. 8. The cooling rate of the freeze box in the first half hour is approximately 0.83 °C/min and the temperature gradually reaches approximately − 20 °C in 6 h. Then, the internal temperature of the freeze box naturally increases to approximately 20 °C in the air-conditioned room in 6 h. The internal temperature of the red sandstone samples has the same change trend. However, there is a stable stage of the red sandstone temperature near 0 °C, because a large amount of heat is released due to water freezing at this point. The duration of this stable stage near 0 °C becomes much longer with an increasing water content. In addition, the cooling and heating rates of the red sandstone with high saturation are also slower than those of the red sandstone with low water saturation. This illustrates that the water content has a significant influence on the internal temperature distribution of the samples. In addition, it should be noted that the cooling process of the compensation block is also not equal to that of the measured samples. Thus, the synchronous compensation and correction of frost heave may be unreasonable. This is why the strain correction in Sect. 2.3 is based on the premise of an equal temperature instead of an equal time.
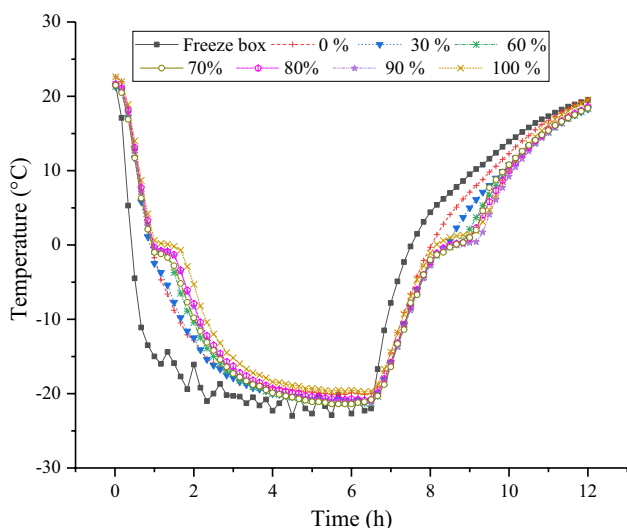

Fig. 8 The temperature inside the red sandstone during freeze–thaw process

3.2 The Influence of Water Saturation on the Frost Deformation and Damage

The frost heaving strains of red sandstone with different water contents are shown in Fig. 9. This shows that the water content has a significant influence on the frost heaving of the red sandstone. With an increasing water content, the total strain of this red sandstone changes from shrinkage to expansion at low temperatures. When the degree of water saturation is less than 85%, the total deformation of the red sandstone is dominated by shrinkage, although there is a temporary expansion process below the freezing point (approximately 0 °C) to offset some of the shrinkage deformation. Beyond 85% water saturation, obvious frost heaving strain occurs at low temperatures. The total frost heaving strain is greater than 2000×10^{-6} when $S_r = 100\%$. The peak frost heaving strain and residual strain also rapidly increase beyond 85% water saturation, while they are almost zero below 85% water saturation (Figs. 10, 11).

There are specifically three types of typical deformation and damage characteristics for the red sandstone according to the water content.

(1) $S_r = 0\%$

The completely dry red sandstone linearly shrinks with decreasing freezing temperature. There is no expansion deformation during the entire freeze–thaw process, and the shrinkage of this sample is only caused by the contraction of the rock matrix during freezing. Because there is a lack of pore water, the peak frost heaving strain and the residual strain are almost zero (Figs. 10, 11). The amplitude of every AE activity and cumulative AE energy for the red sandstone samples under one freeze–thaw cycle are plotted in Fig. 12a. The changes in the trends of AE activities can be used to predict the rock deformation and the generation of microcracks, especially microcrack development and evolution inside the rock (Kong et al. 2016). This shows that few AE activities are observed for the completely dry red sandstone samples. Therefore, little damage occurs under this condition.

(2) $S_r = [30\%, 85\%]$

The frost deformation includes the thermal shrinkage of the rock matrix caused by the temperature reduction and the frost heave of pores caused by the pore ice pressure. However, the total deformation of the unsaturated red sandstone with a water saturation less than 85% is always shrinkage at low temperatures, because the frost heaving strain is too small to resist thermal shrinkage during the cooling process. In fact, when the ice pressure builds up inside the porous network, the excess liquid will be expelled from the freezing sites. If there are too many empty pores in the red sandstone sample, then
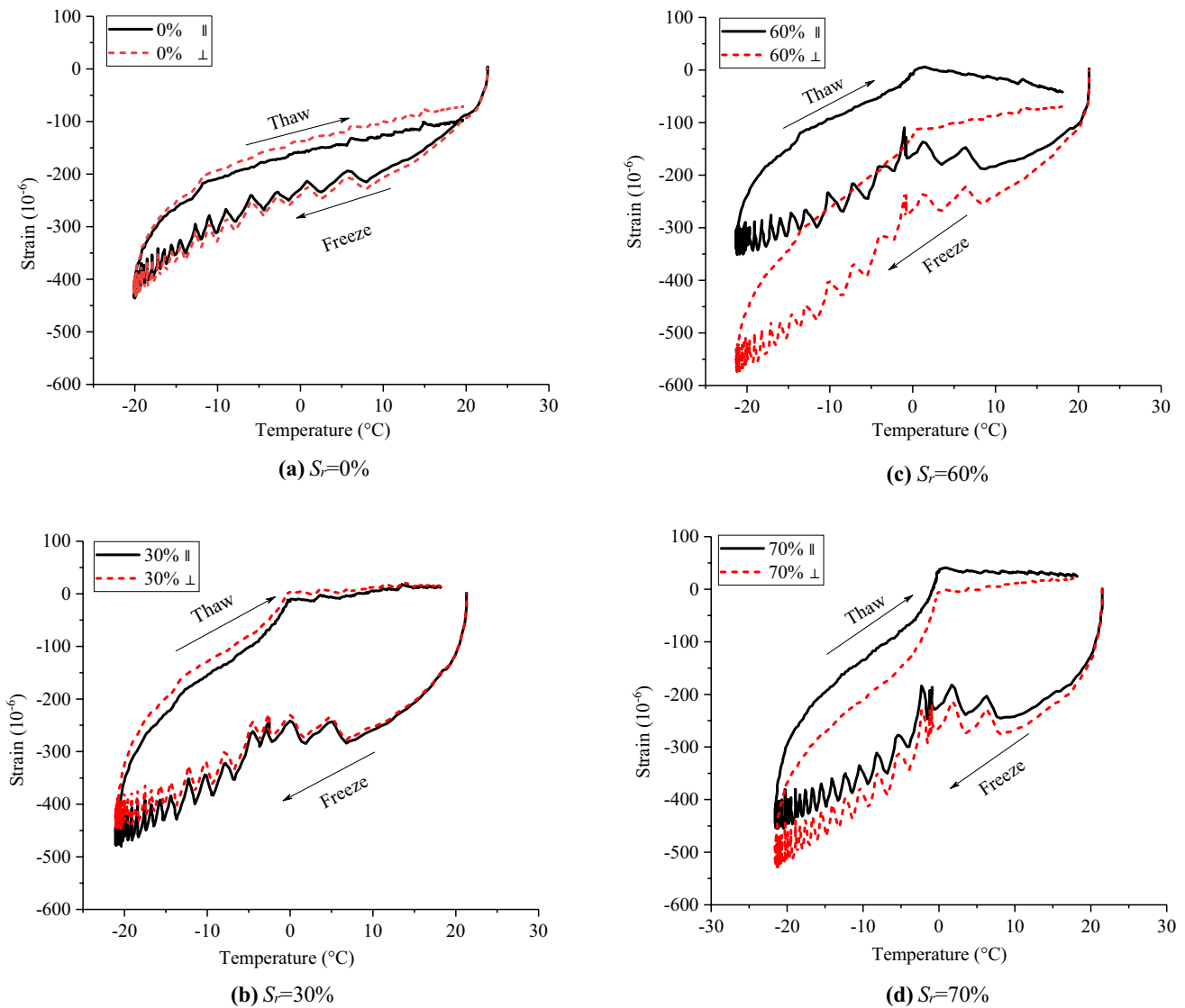
Fig. 9 The influence of water saturation on the frost deformation of red sandstone ('‖' and '⊥' represent the directions parallel and vertical to the axis of the cylindrical samples, respectively)

the ice pressure will be released as the excess liquid in saturated pores is expelled into unsaturated pores during freezing (Coussy and Monteiro 2007). Therefore, the peak frost heaving strain is close to zero, as is the residual strain of this sandstone after thawing (Figs. 10, 11). This illustrates that the frost damage is very small and that the freeze–thaw action does not cause any significant plastic strain below 85% water saturation. In addition, the AE activities also increase with the increase of water saturation for these unsaturated red sandstones from 106 AE activities to 192 AE activities (Fig. 12b–e). The cumulative AE energy has the same change trend (Fig. 13). However, the AE amplitude and AE energy are still very small below 85% water saturation. The AE activities and the residual strains show

that the damage caused by one freeze–thaw cycle may be ignored for red sandstone with a water saturation less than 85%.

(3) $S_r = [85\%, 100\%]$.

Beyond 85% water saturation, obvious frost heaving strain occurs when the temperature falls below the freezing point (approximately 0 °C). The total deformation changes from freezing shrinkage to frost heave. Both the peak frost heaving strain after freezing and the residual strain after thawing increase quickly beyond this critical water saturation of 85% (Figs. 10, 11). The irreversible residual strain reflects the freeze–thaw damage degree of red sandstone (Wang et al. 2020). Therefore, more serious freeze–thaw damage will be
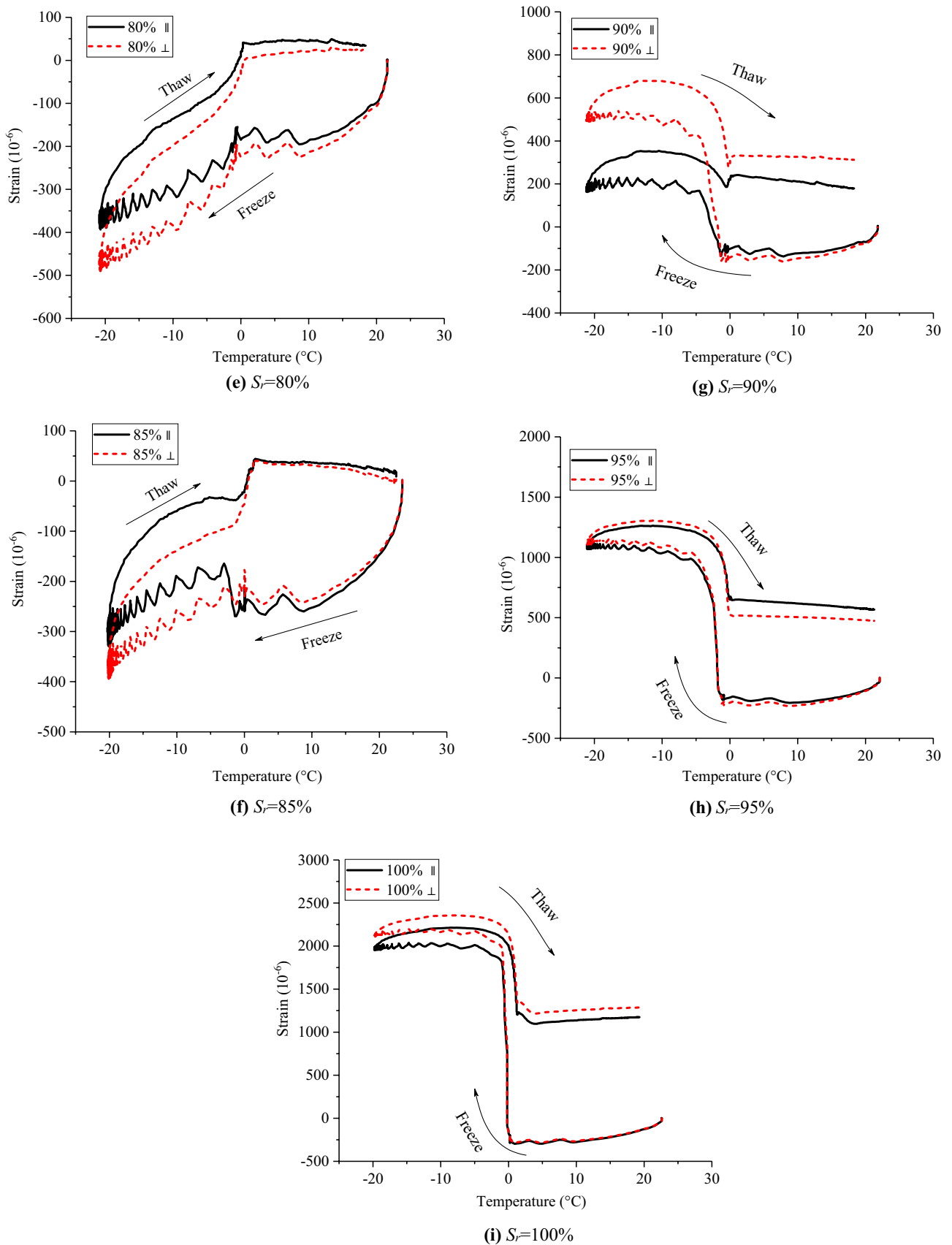
(e) S_r=80%
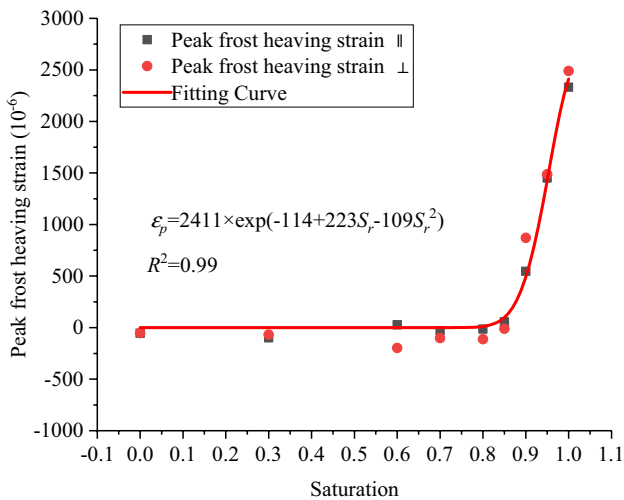

(g) S_r=90%

(f) S_r=85%

(h) S_r=95%

(i) S_r=100%

Fig. 9 (continued)

Fig. 10 The peak frost heaving strains of red sandstone after freezing with different water saturations at $-20\ °C$ (the thermal contraction of the rock matrix was subtracted, about 376×10^{-6})
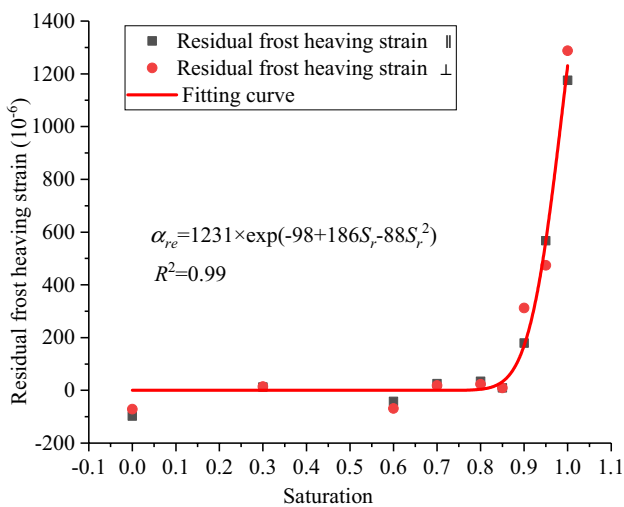

Fig. 11 The residual frost heaving strains of red sandstone with different water saturations after thawing at $20\ °C$

produced in red sandstone with high water saturations. The freezing expansion of pores induced by pore ice pressure should be responsible for this damage since there are not enough empty voids to store the expansive volume of freezing water (Huang et al. 2018b, 2019b). A rapid increase in AE activity also occurs in the red sandstone with high water saturations beyond 85% (Fig. 12f–g). Both the AE activities and the cumulative AE energy and AE amplitude exhibit considerable growth. In addition, an interesting phenomenon is the concentrated presence of AE activities near 0 °C, because a large amount of pore water freezes around this freezing point. The AE activity is a direct index of the

intensity of internal microcracks (Meng et al. 2018). A large number of AE events indicate that microcracks are experiencing substantial growth and that freeze–thaw damage near this freezing point plays a major role. In addition, the test results show that most of the AE activities arise during the freezing process. Therefore, the freeze–thaw damage of the high-saturation red sandstone is mainly caused by the freezing expansion of pores rather than the thermal deformation of rock matrix, and most of the freezing expansion of pores in this red sandstone occurs near 0 °C.

The experimental results of the peak and residual strains show exponential growth. Considering the boundary conditions, the following exponential function may be used to quantify the relationship between the peak strain and the water saturation:

$$\varepsilon_{\mathrm{p}} = \varepsilon_{\mathrm{p}}^{\mathrm{sa}} \exp(a_1 S_{\mathrm{r}}^2 + b_1 S_{\mathrm{r}} - a_1 - b_1), \tag{8}$$

where $\varepsilon_{\mathrm{p}}^{\mathrm{sa}}$ is the peak frost heaving strain. For this red sandstone, $\varepsilon_{\mathrm{p}}^{\mathrm{sa}} = 2411 \times 10^{-6}$ is determined experimentally, S_{r} is the degree of water saturation, and a_1 and b_1 are unknown parameters that need to be determined by the experimental results of the peak frost heaving strains with different water saturations.

Similarly, this exponential function can also be used to quantify the relationship between the residual strain and the water saturation after thawing:

$$\varepsilon_{\mathrm{re}} = \varepsilon_{\mathrm{re}}^{\mathrm{sa}} \exp(a_2 S_{\mathrm{r}}^2 + b_2 S_{\mathrm{r}} - a_2 - b_2), \tag{9}$$

where $\varepsilon_{\mathrm{re}}^{\mathrm{sa}}$ is the residual strain. For this red sandstone, $\varepsilon_{\mathrm{re}}^{\mathrm{sa}} = 1231 \times 10^{-6}$ is determined experimentally, and a_2 and b_2 are unknown parameters that need to be determined by the experimental results of the residual strains with different water saturations.

By fitting the experimental results shown in Figs. 10 and 11, the functions of the peak frost heaving strain and the residual strain against the water saturation during one freeze–thaw cycle can be expressed as follows:

$$\varepsilon_{\mathrm{p}} = 2411 \exp(-109 S_{\mathrm{r}}^2 + 223 S_{\mathrm{r}} - 114), \tag{10}$$

$$\varepsilon_{\mathrm{re}} = 1231 \exp(-88 S_{\mathrm{r}}^2 + 186 S_{\mathrm{r}} - 98). \tag{11}$$

4 Proposed Frost Heaving Model for Unsaturated Red Sandstone

Generally, the total strain mainly includes the thermal shrinkage strain of the rock matrix caused by the decrease in temperature and the frost heaving strain caused by the ice pressure in pores:
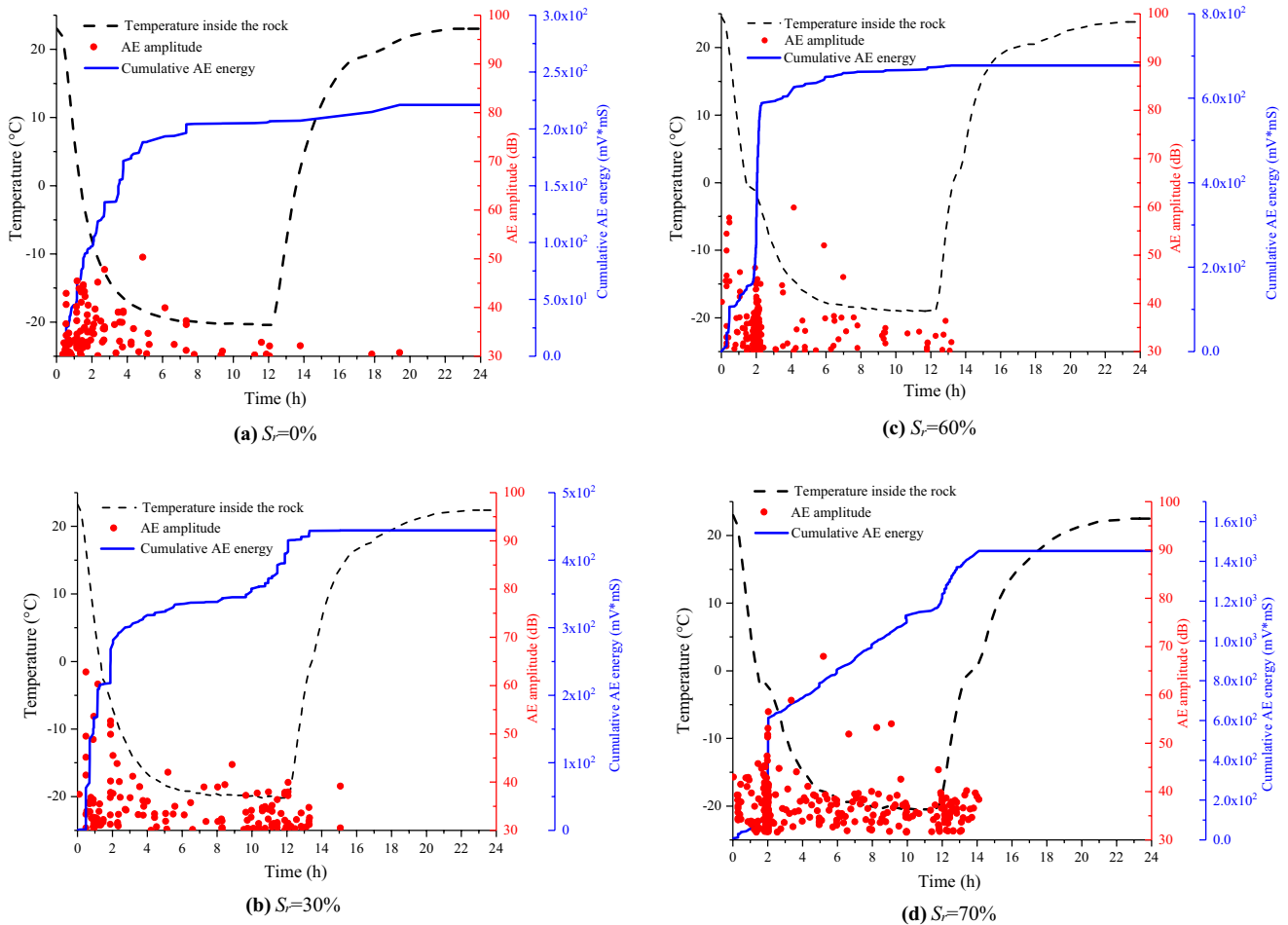
Fig. 12 The AE activities during one freeze–thaw cycle for red sandstone with different water saturations

$$\varepsilon = \varepsilon_T + \varepsilon_f, \tag{12}$$

where

$$\varepsilon_T = \alpha_r(T - T_0), \tag{13}$$

$$\varepsilon_f = b\frac{p_i}{3K_r}, \tag{14}$$

where K_r is the bulk modulus of red sandstone. ε_T is the linear thermal strain, ε_f is the linear frost heaving strain caused by ice pressure, and b is the Biot coefficient of the red sandstone.

According to the theory of micromechanics (Dormieux et al. 2006), the Biot coefficient can be written as

$$b = \frac{n(3K_r + 4G_r)}{3K_r n + 4G_r}. \tag{15}$$

Substituting Eqs. (13) and (14) into Eq. (12), the total strain is

$$\varepsilon = \alpha_r \delta T + b\frac{p_i}{3K_r}. \tag{16}$$

According to the saturated frost heaving model based on the assumption of spherical pores (Fig. 14), the equivalent pore ice pressure in saturated frozen red sandstone can be expressed as (Huang et al. 2018c)

$$p_i^s = \begin{cases} \dfrac{0.029[1-w_u(T)]}{\frac{2(1-2v_r)}{(2-3n)-(4-3n)v_r}\frac{1+2n+(1-4n)v_r}{2(1-n)}\frac{1}{E_r}+1.029\frac{1-2v_i}{E_i}}\delta_{ij} & \Delta T \leq 0 \\ 0 & \Delta T > 0 \end{cases}, \tag{17}$$

where p_i^s is the equivalent pore ice pressure in the saturated red sandstone, E_r and v_r are the elastic modulus and Poisson's ratio of sandstone, E_i and v_i are the elastic modulus and Poisson's ratio of solid ice, respectively, and $\Delta T = T - T_m$. T_m is the freezing point of bulk water, and $w_u(T)$ is the unfrozen water content.

The equivalent pore ice pressure is significantly influenced by the unfrozen water content, because only the frozen water can contribute to the ice pressure. The
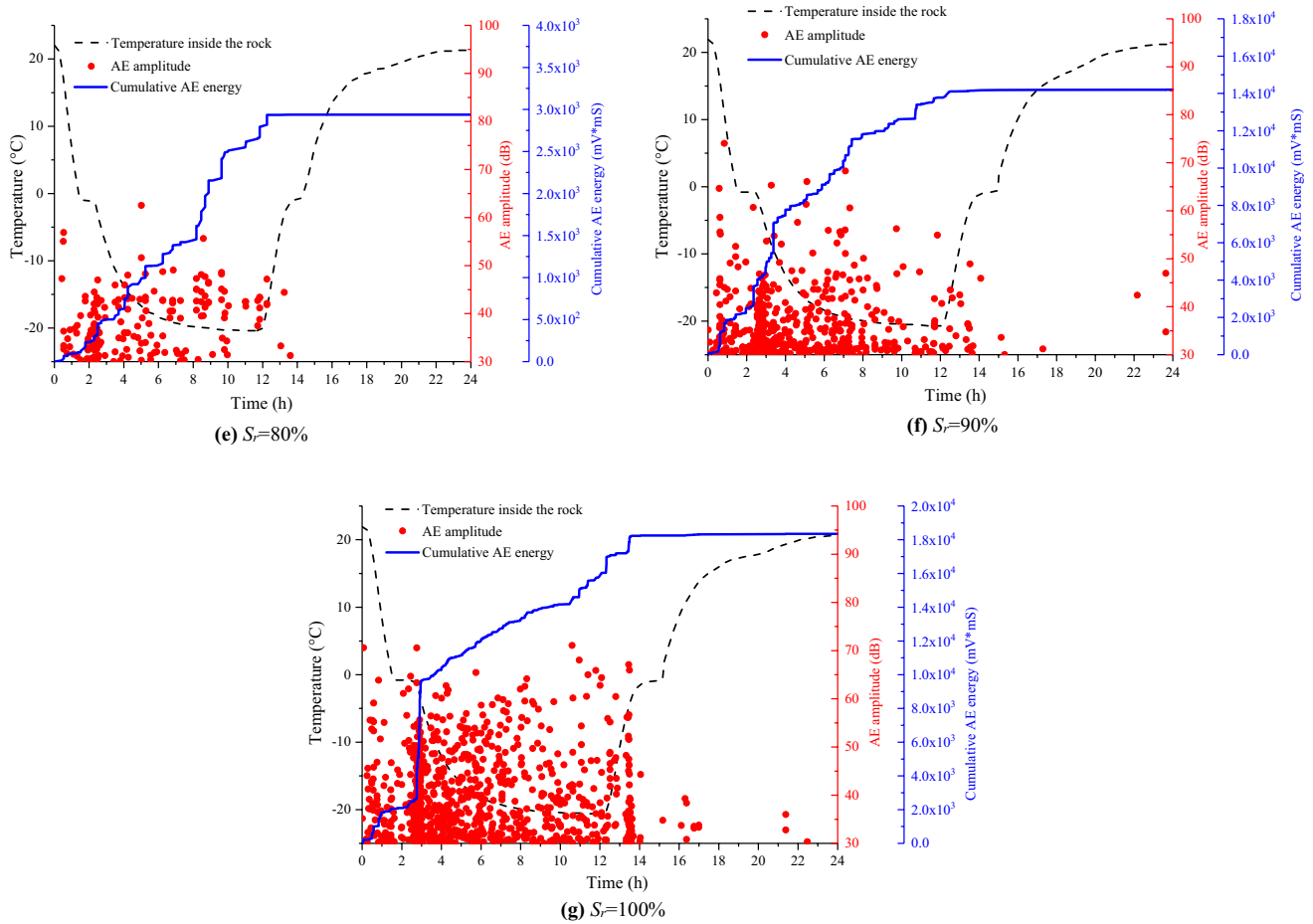
Fig. 12 (continued)

unfrozen water content $w_u(T)$ depends on the pore size distribution and the freezing temperature. For sandstone,

Fig. 13 The relationship between the cumulative AE energy and the water saturation during one freeze–thaw cycle for the red sandstone

a dual-porosity function can be adopted to express the unfrozen water content (Huang et al. 2018c, 2019a):

$$w_u(T) = \begin{cases} 1 - F(r_c) & \Delta T \leq 0 \\ 1 & \in \Delta T > 0 \end{cases}, \quad (18)$$

where

$$F(r) = 1 - [V_1 \exp(m_1/r) + V_2 \exp(m_2/r)], \quad (19)$$

where $F(r)$ is the cumulative distribution function of pore size for the sandstone using the dual-porosity model, r is the radius of sphere pores, m_1 and m_2 are the characteristic size of coarse pores and thin pores, respectively, V_1 and V_2 are the volume fractions of coarse and thin pores, respectively, $V_1 + V_2 = 1$, and m_1, m_2, V_1 and V_2 are determined by fitting the cumulative distribution of the pore size.

According to the Gibbs–Thomson equation, the relationship between the critical pore size r_c and the freezing temperature T can be expressed as (Wu et al. 2002)
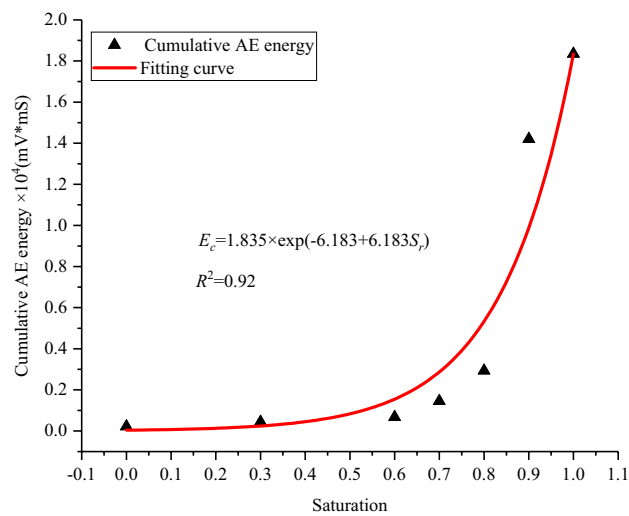
Fig. 14 The schematic diagram of frost heaving model for spherical pores

$$r_{\mathrm{c}} = \frac{2\gamma_{\mathrm{il}}}{\Delta T \rho_{\mathrm{i}} \ell} T_{\mathrm{m}}. \tag{20}$$

Substituting Eq. (20) into Eq. (19), yields

$$F(r_{\mathrm{c}}) = 1 - [V_1 \exp(M_1 \Delta T) + V_2 \exp(M_2 \Delta T)], \tag{21}$$

where r_{c} is the critical radius of spherical pores. This means that only the liquid water in the pores with radii larger than r_{c} will freeze when the temperature drops to T. $M_1 = \frac{m_1 \rho_{\mathrm{i}} \ell}{2\gamma_{\mathrm{il}} T_{\mathrm{m}}}$, $M_2 = \frac{m_2 \rho_{\mathrm{i}} \ell}{2\gamma_{\mathrm{il}} T_{\mathrm{m}}}$, ρ_{i} is the density of solid ice, γ_{il} is the ice-liquid interfacial free energy, and ℓ is the latent heat per unit mass of water.

The equivalent pore ice pressure is much smaller in unsaturated rock. Introducing an impact coefficient $\xi(S_{\mathrm{r}})$, the influence of water saturation on the equivalent pore ice pressure can be expressed as

$$p_{\mathrm{i}} = \xi(S_{\mathrm{r}})p_{\mathrm{i}}^{\mathrm{s}}. \tag{22}$$

Substituting Eq. (22) into Eq. (16), the total strain of freezing unsaturated sandstone can be written as

$$\varepsilon = \alpha_{\mathrm{r}}(T - T_0) + \xi(S_{\mathrm{r}})\varepsilon_{\mathrm{sa}}, \tag{23}$$

where $\varepsilon_{\mathrm{sa}} = b\frac{p_{\mathrm{i}}^{\mathrm{s}}}{3K_{\mathrm{r}}}$ is the frost heaving strain of the red sandstone with 100% water saturation.

By conducting MIP and BET tests, the cumulative pore volume fraction against the pore size can be derived, as shown in Fig. 15. The unknown parameters m_1 and m_2 in Eq. (19) are determined by fitting the experimental results of the pore size distribution (Fig. 15). Then, the values of M_1 and M_2 in Eq. (21) can also be determined. The unfrozen water content in this red sandstone with 100% water saturation can be obtained by substituting Eq. (21) into Eq. (18) as shown in Fig. 16. It can be found that all the pore water freezes at -20 °C, because the pores in this red sandstone are larger than the critical freezing radius
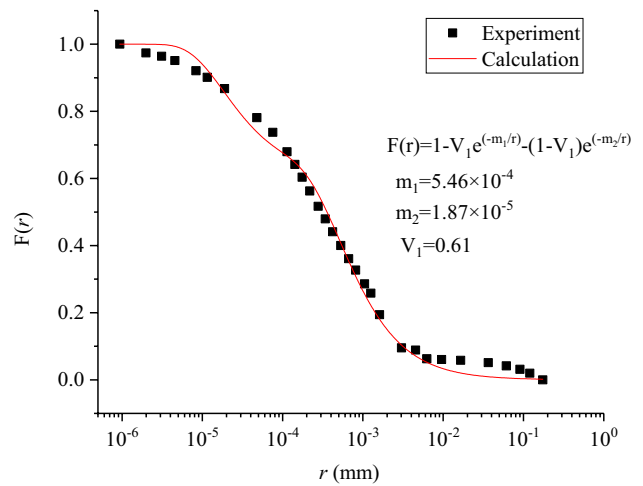

$F(r) = 1 - V_1 e^{(-m_1/r)} - (1-V_1)e^{(-m_2/r)}$
$m_1 = 5.46 \times 10^{-4}$
$m_2 = 1.87 \times 10^{-5}$
$V_1 = 0.61$

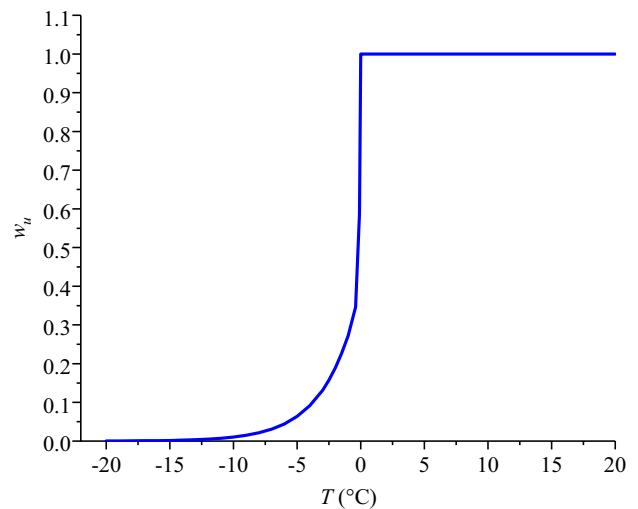**Fig. 15** Cumulative pore volume fraction of the red sandstone

Fig. 16 The unfrozen water content in saturated red sandstone against the freezing temperature
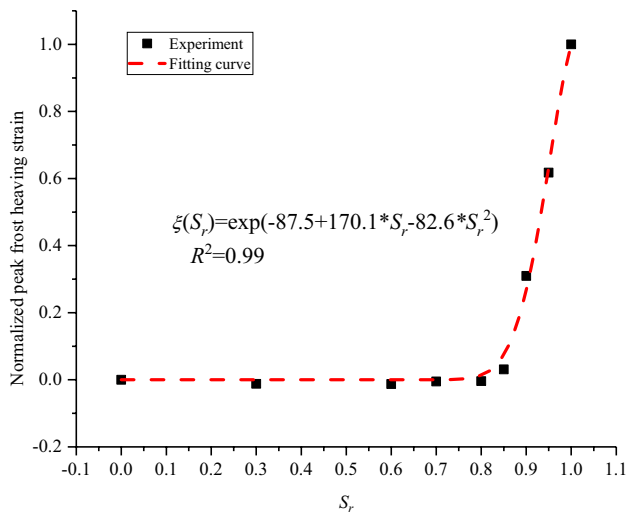
Fig. 17 The normalized peak frost heaving strains against water saturations

(2.58 nm at − 20 °C) according to the measured pore size distribution.

To derive the expression of the impact coefficient $\xi(S_r)$ of water saturation, the peak frost heaving strains in Fig. 10 are normalized from 0 to 1. Then, $\xi(S_r)$ can be obtained by fitting the normalized experimental values as follows (Fig. 17):

$$\xi(S_r) = \exp(-87.5 + 170.1 S_r - 82.6 S_r^2). \quad (24)$$

Substituting Eqs. (17), (18), (21), (24) and the values of the parameters in Tables 1 and 3 into Eq. (23), the final total strain of this red sandstone at different freezing temperatures is

heaving model can be used to accurately predict the frost deformation of red sandstone with different water contents. It should be noted out that although the peak and residual strains during freezing and thawing are dependent on the rock types, the present model can also be used to predict the frost deformation of other rocks. For different rocks, Eq. (24) should be determined by fitting the experimental results of the specified rocks with different water saturations, then the predicted deformation can be estimated using Eq. (23).

5 Discussion

In this research, the experimental results showed that 85% may be a critical saturation for the red sandstone samples, beyond which the deformation changed from frost shrinkage to frost heave at low temperatures. A similar critical degree of water saturation ($S_r = 85\%$) was found for both tuffeau and Richemont limestone by Al-Omari et al. (2015), which suggests that a threshold limit of moisture content exists. The AE activities and residual frost heaving strain further confirm this critical value. The low-saturation sandstone (water saturation below 85%) suffers little freeze–thaw damage. All the frost heaving strains are recovered and the accumulated AE energy is small after one freeze–thaw cycle for the low-saturation sandstone. Therefore, the water content is an important factor influencing the freeze–thaw damage degree. For rock engineering in cold regions, the existence of a critical saturation threshold provides inspiration for a waterproof design to prevent freeze–thaw damage to rocks (Lai et al. 2016). In addition, the cumulative energy of AE activities

$$\varepsilon = \begin{cases} \{9.4(T - T_0) + 2295 e^{(-87.5 + 170.1 S_r - 82.6 S_r^2)}(0.61\, e^{10.6\Delta T} + 0.39\, e^{0.36\Delta T})\} \times 10^{-6} & \Delta T \le 0 \\ 9.4 \times 10^{-6}(T - T_0) & \Delta T > 0 \end{cases}. \quad (25)$$

For Eq. (25), the first item is the thermal strain, and the second item is the frost heaving strain considering the influence of the water saturation and unfrozen water content.

The calculated results of the frost heaving strains are compared with the experimental values for the red sandstone with different water contents, as shown in Fig. 18, which shows good consistency. Beyond 85% water saturation, the red sandstone experiences obvious frost heaving deformation at low temperatures. The proposed frost

may be a potential indicator for quantifying the freeze–thaw damage and predicting the freeze–thaw rupture locations in rocks (Amitrano et al. 2012; Girard et al. 2013). Nondestructive monitoring technologies, including frost deformation and AE signal measurements, are well applied to investigate the influence of water saturation on the freeze–thaw damage of red sandstone by laboratory experiments. However, further research is required to reveal the long-term freeze–thaw damage mechanism of unsaturated sandstone.

Table 3 The physico-mechanical parameters of the water/ice medium (Watanabe and Mizoguchi 2002; Lide 2004; Huang et al. 2018c)

ρ_i (kg/m³)	ρ_l (kg/m³)	E_i (GPa)	μ_i	ℓ (m². ⁻²)	T_m (°C)	γ_{il} (N/m)
917	1000	8.348	0.325	334.88×10³	0	0.029

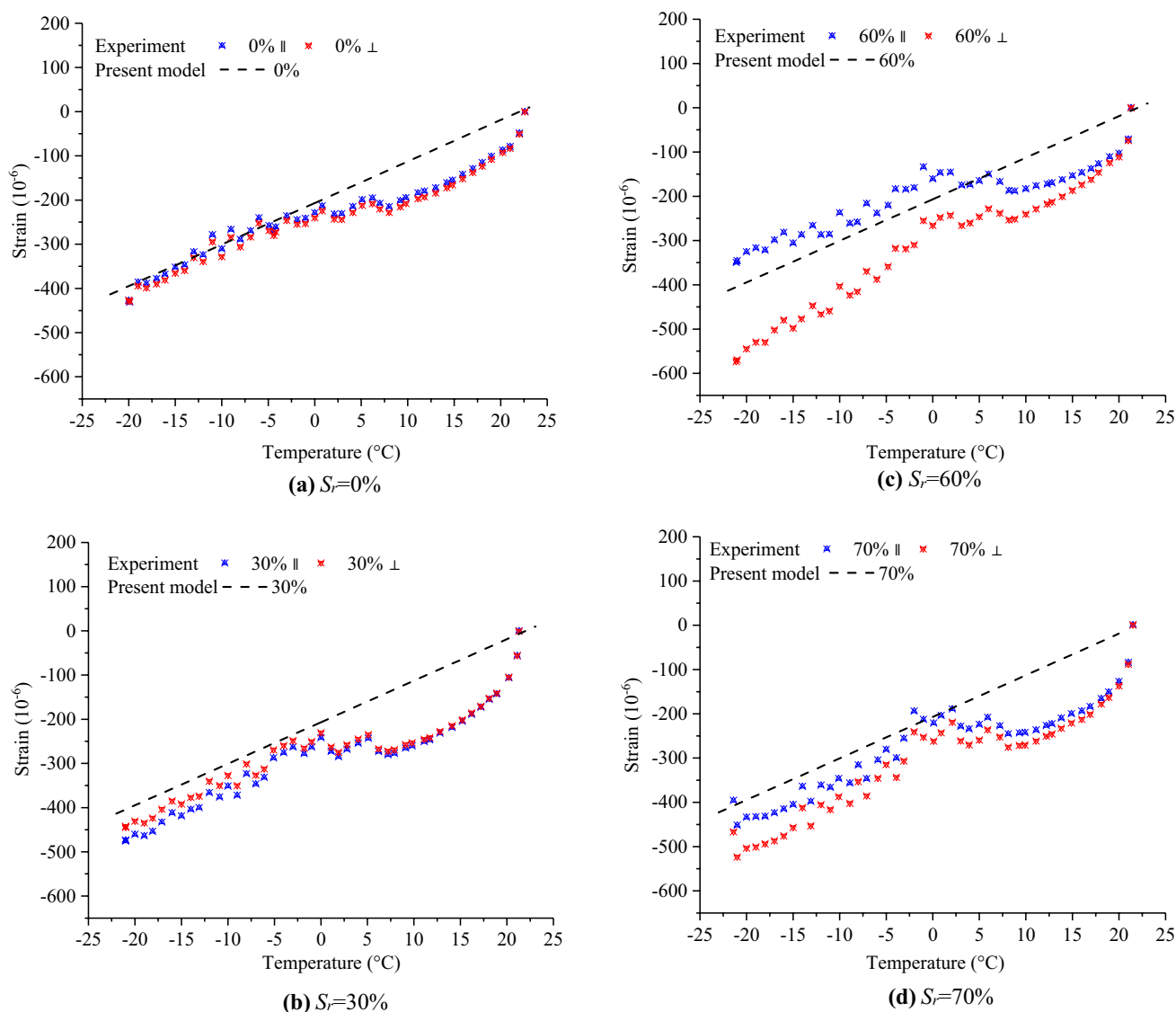**Fig. 18** The calculated strains versus the experimental strains for the freezing red sandstone with different water saturations ('∥' and '⊥' represent the directions parallel and vertical to the axis of the cylindrical samples, respectively)

(1) The stability and reliability of the long-term frost deformation measurement using strain gauges.

It should be noted that there is little difference between the calculated curves and the experimental values of the total strain in the initial cooling stage (Fig. 18). The fast decrease in the experimental strains in the initial cooling stage is caused by rapid cooling. This illustrates that the strain gauges and the 704 glue are sensitive to the cooling rate. Due to the sensitivity of the strain gauges, the experimental strain is always volatile under cooling, as shown in Fig. 9. The long-term stability and reliability of this measurement method during freeze–thaw cycles should be investigated. In previous studies, 704 glue and special adhesive glue were usually applied to the strain gauges (Fang and Huang 2019). However, research of their low-temperature properties is insufficient. As a preliminary investigation, their long-term properties were tested in this study to ensure the strain gauges continued to adhere reliably and tightly under freeze–thaw conditions (Fig. 19). The measured frost strains have a decreasing trend after seven freeze–thaw cycles when only the special adhesive glue was used, because the special adhesive glue broke away from the red sandstone after repeated freeze–thaw cycles. Therefore, the proposed adhesion method of the strain gauges in this research is much better, 704 glue should be used first to prevent the interior water of the red sandstone from escaping (Fig. 5). Regardless, the low-temperature sensitivity of the strain gauge and glue should be further confirmed.
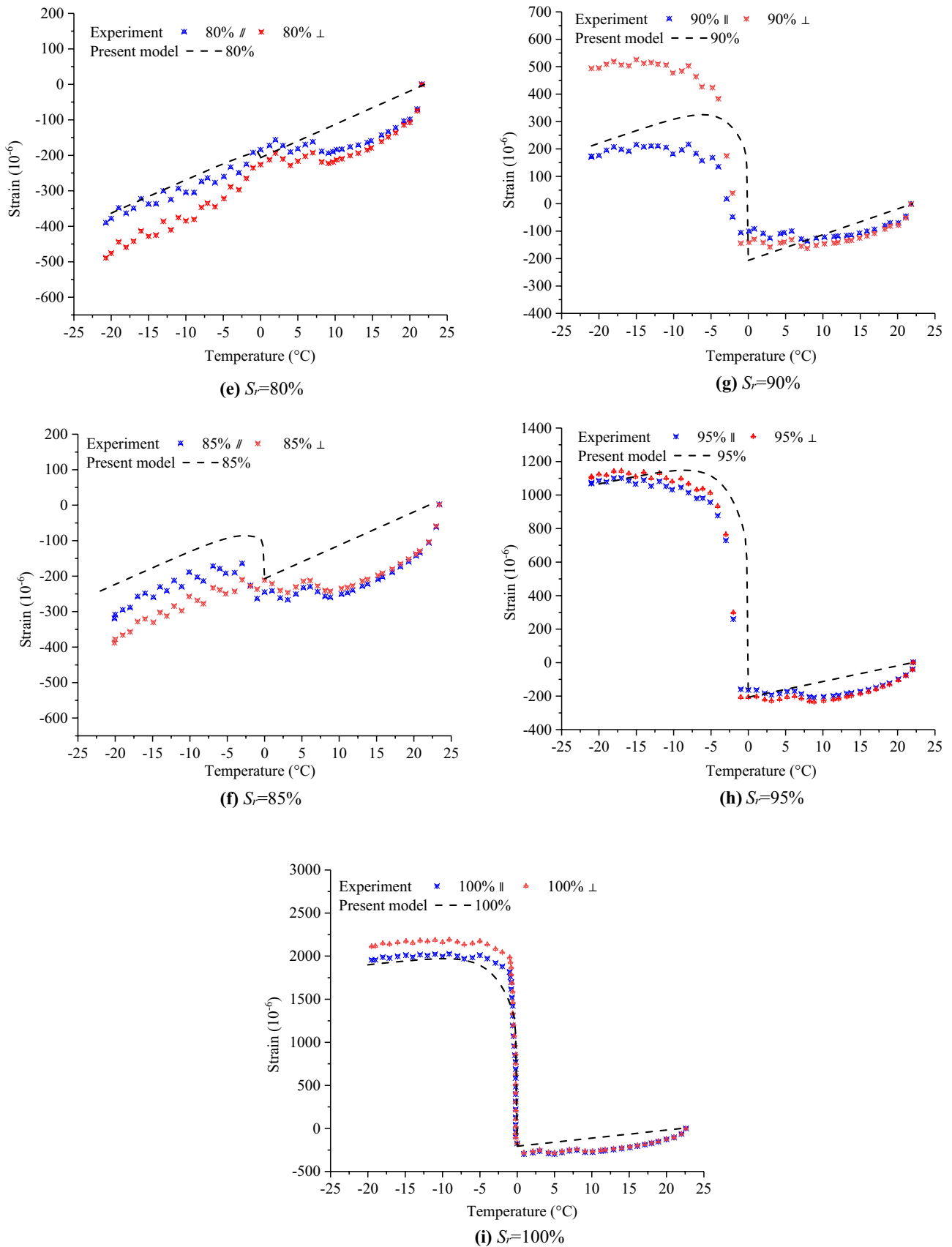
(e) S_r=80%

(g) S_r=90%

(f) S_r=85%

(h) S_r=95%
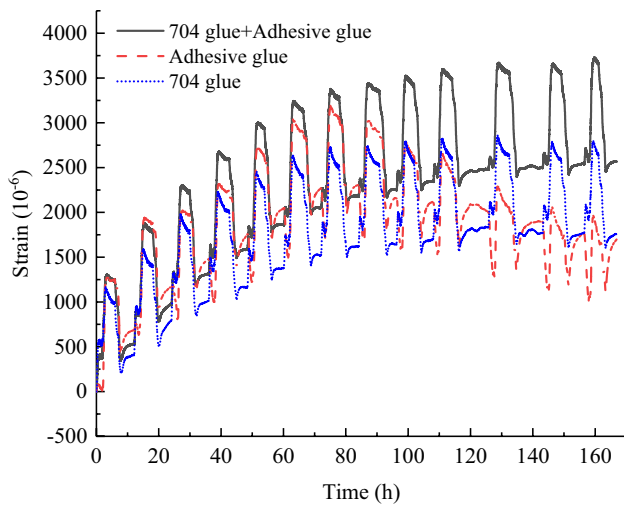
(i) S_r=100%

Fig. 18 (continued)

Fig. 19 Comparison of the glue stability and reliability for the long-term frost deformation measurement using strain gauges
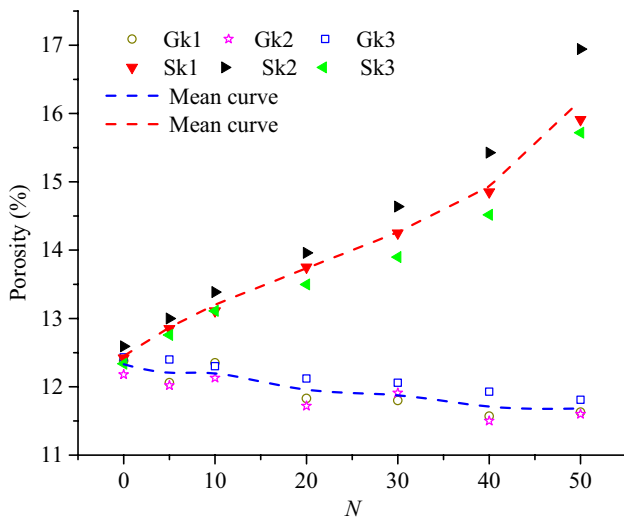

Fig. 20 Comparison of the porosities between fully saturated and dried red sandstones under freeze–thaw conditions (Sk1, Sk2, Sk3 are fully saturated samples and Gk1, Gk2, Gk3 are dried samples) (Liu et al. 2020)

(2) The influence of water saturation on the long-term freeze–thaw damage of rocks.

With an increasing number of freeze–thaw cycles, the pore size and porosity also increase. Therefore, more and more voids will be produced to store the expansive volumes caused by water freezing. The change trends of porosities under freeze–thaw cycles show that the long-term freeze–thaw damage is much more serious in saturated red sandstone than in dry red sandstone (Fig. 20). A rapid increase in the porosity after 40 freeze–thaw cycles for the saturated sandstone

is caused by the production of freeze–thaw cracks. The long-term monitoring of frost deformation and AE activities is very important for explaining the long-term frost resistance of rock with different water contents. In this study, the influence of the water saturation on the freeze–thaw damage of red sandstone is limited to one freeze–thaw cycle. Therefore, the influence of the water saturation on the change law of the long-term freeze–thaw damage needs further quantitative research.

(3) The influence of the confining pressure on the frost deformation and freeze–thaw damage of unsaturated rocks.

At present, frost deformation and freeze–thaw damage are studied in the absence of the confining pressure (Lv et al. 2019; Huang et al. 2020a, b). However, engineering rocks in cold regions are located in an in situ stress field. Generally, the presence of a confining pressure can improve the strength of sandstone after freeze–thaw cycles (Zhang et al. 2020). From the aspect of frost deformation, the confining pressure will restrict the frost expansion of rock samples during pore water freezing. However, when the confining pressure is applied, the pore frost heaving pressure may increase because the confined effect of the pore wall on the freezing pore water will be strengthened. Therefore, the frost deformation and freeze–thaw damage characteristics are different when the confining pressure is considered. Liu et al. (2019) claimed that the freeze–thaw damage of water-rich sandstone increased with an increasing confining pressure by testing the pore size distribution with a CT (computed tomography) scanner. They found that the measured increment in the porosity after freeze–thaw action was much larger under a high confining pressure. However, the influence of the confining pressure on the frost deformation and freeze–thaw damage of unsaturated rocks requires more experimental evidence.

6 Conclusion

The frost deformation of red sandstone is an exponential function of the water saturation. The experimental results show that remarkable frost heaving strain and residual strain will occur, only when the water saturation exceeds 85%. Therefore, 85% is a critical saturation value for this red sandstone under freeze–thaw cycles.

AE activities also increase with increasing water saturation for this red sandstone. The cumulative AE energy has the same change trend as the frost heaving strain, and thus, the cumulative AE energy is also a great indicator for determining the freeze–thaw damage degree. However, AE activities only occur in the freezing process. Therefore,

freeze–thaw damage is mainly caused by frost heave during freezing rather than thawing shrinkage.

The frost deformation of red sandstone is related to the water saturation and the pore size distribution. Considering these two influencing factors, the developed frost heaving model based on pore micromechanics theory can be used to accurately predict the frost deformation of unsaturated red sandstone.

Declarations

Conflict of interest The authors declared that they have no conflicts of interest to this work.

References

Al-Omari A, Beck K, Brunetaud X, Török Á, Al-Mukhtar M (2015) Critical degree of saturation: a control factor of freeze–thaw damage of porous limestones at Castle of Chambord, France. Eng Geol 185:71–80

Amitrano D, Gruber S, Girard L (2012) Evidence of frost-cracking inferred from acoustic emissions in a high-alpine rock-wall. Earth Planet Sci Lett 341:86–93

Binal A (2009) A new laboratory rock test based on freeze–thaw using a steel chamber. Q J Eng Geol Hydrogeol 42(2):179–198

Chen TC, Yeung MR, Mori N (2004) Effect of water saturation on deterioration of welded tuff due to freeze–thaw action. Cold Reg Sci Technol 38(2–3):127–136

Coussy O, Monteiro P (2007) Unsaturated poroelasticity for crystallization in pores. Comput Geotech 34(4):279–290

Dormieux L, Kondo D, Ulm FJ (2006) Microporomechanics. Wiley

Eslami J, Walbert C, Beaucour AL, Bourges A, Noumowe A (2018) Influence of physical and mechanical properties on the durability of limestone subjected to freeze–thaw cycles. Constr Build Mater 62:420–429

Fang T, Huang M (2019) Deformation and load-bearing characteristics of step-tapered piles in clay under lateral load. Int J Geomech 19(6):04019053

Fang W, Jiang N, Luo X (2019) Establishment of damage statistical constitutive model of loaded rock and method for determining its parameters under freeze–thaw condition. Cold Reg Sci Technol 160:31–38

Freire-Lista DM, Fort R, Varas-Muriel MJ (2015) Freeze–thaw fracturing in building granites. Cold Reg Sci Technol 113:40–51

Fu HL, Zhang JB, Huang Z, Shi Y, Chen W (2018) A statistical model for predicting the triaxial compressive strength of transversely isotropic rocks subjected to freeze–thaw cycling. Cold Reg Sci Technol 145:237–248

Girard L, Gruber S, Weber S, Beutel J (2013) Environmental controls of frost cracking revealed through in situ acoustic emission measurements in steep bedrock. Geophys Res Lett 40(9):1748–1753

Hori M, Morihiro H (1998) Micromechanical analysis on deterioration due to freezing and thawing in porous brittle materials. Int J Eng Sci 36(4):511–522

Hu Z, Ding H, Lai J, Wang H, Wang X, He S (2018) The durability of shotcrete in cold region tunnel: a review. Constr Build Mater 185:670–683

Huang SB, Liu QS, Cheng AP, Liu YZ (2018a) A statistical damage constitutive model under freeze–thaw and loading for rock and its engineering application. Cold Reg Sci Technol 145:142–150

Huang SB, Liu QS, Liu YZ, Kang YS, Cheng AP, Ye ZY (2018b) Frost heaving and frost cracking of elliptical cavities (fractures) in low-permeability rock. Eng Geol 234:1–10

Huang SB, Liu QS, Liu YZ, Ye ZY, Cheng AP (2018c) Freezing strain model for estimating the unfrozen water content of saturated rock under low temperature. Int J Geomech 18(2):04017137

Huang SB, Liu QS, Liu YZ, Ye ZY, Cheng AP (2019a) Closure to "freezing strain model for estimating the unfrozen water content of saturated rock under low temperature" by Shibing Huang, Quansheng Liu, Yanzhang Liu, Zuyang Ye, and Aiping Cheng. Int J Geomech 19(7):07019002

Huang SB, Liu YZ, Guo YL, Zhang ZL, Cai YT (2019b) Strength and failure characteristics of rock-like material containing single crack under freeze–thaw and uniaxial compression. Cold Reg Sci Technol 162:1–10

Huang SB, Zexin Lu, Ye ZY, Xin ZK (2020a) An elastoplastic model of frost deformation for the porous rock under freeze–thaw. Eng Geol 278:105820. https://doi.org/10.1016/j.enggeo.2020.105820

Huang SB, Ye YH, Cui XZ, Cheng AP, Liu GF (2020b) Theoretical and experimental study of the frost heaving characteristics of the saturated sandstone under low temperature. Cold Reg Sci Technol 174:103016. https://doi.org/10.1016/j.coldregions.2020.103036

Huang SB, He YB, Liu GF, Lu ZX, Xin ZK (2021) Effect of water content on the mechanical properties and deformation characteristics of the clay-bearing red sandstone. B Eng Geol Environ. https://doi.org/10.1007/s10064-020-01994-6

Jia HL, Xiang W, Krautblatter M (2015) Quantifying rock fatigue and decreasing compressive and tensile strength after repeated freeze-thaw cycles. Permafrost Periglac 26(4):368–377

Jia HL, Zi F, Yang GS, Li GY, Shen YJ, Sun Q, Yang PY (2020a) Influence of pore water (ice) content on the strength and deformability of frozen argillaceous siltstone. Rock Mech Rock Eng 53(2):967–974. https://doi.org/10.1007/s00603-019-01943-0

Jia HL, Ding S, Fan Z, Dong YH, Shen YJ (2020b) Evolution in sandstone pore structures with freeze–thaw cycling and interpretation of damage mechanisms in saturated porous rocks. CATENA 195:104915. https://doi.org/10.1016/j.catena.2020.104915

Kong B, Wang E, Li Z, Wang X, Liu J, Li N (2016) Fracture mechanical behavior of sandstone subjected to high-temperature treatment and its acoustic emission characteristics under uniaxial compression conditions. Rock Mech Rock Eng 49(12):4911–4918

Lai J, Qiu J, Fan H, Chen J, Xie Y (2016) Freeze-proof method and test verification of a cold region tunnel employing electric heat tracing. Tunn Undergr Sp Technol 60:56–65

Lide DR (ed) (2004) CRC handbook of chemistry and physics, vol 85. CRC Press

Liu QS, Huang SB, Kang YS, Liu XW (2015) A prediction model for uniaxial compressive strength of deteriorated rocks due to freeze–thaw. Cold Reg Sci Technol 120:96–107

Liu B, Ma Y, Liu N, Han Y, Li D, Deng H (2019) Investigation of pore structure changes in Mesozoic water-rich sandstone induced by freeze–thaw process under different confining pressures using digital rock technology. Cold Reg Sci Technol 161:137–149

Liu YZ, Cai YT, Huang SB, Guo YL, Liu GF (2020) Effect of water saturation on uniaxial compressive strength and damage degree of clay-bearing sandstone under freeze–thaw. B Eng Geol Environ 79:2021–2036

Lu Y, Li X, Chan A (2019) Damage constitutive model of single flaw sandstone under freeze–thaw and load. Cold Reg Sci Technol 159:20–28

Luo XD, Jiang N, Zuo CQ, Dai ZW, Yan ST (2014) Damage characteristics of altered and unaltered diabases subjected to extremely cold freeze–thaw cycles. Rock Mech Rock Eng 47(6):1997–2004

Lv ZT, Xia CC, Li Q, Si ZP (2019) Empirical frost heave model for saturated rock under uniform and unidirectional freezing conditions. Rock Mech Rock Eng 52(3):955–963

Matsuoka N (1990) Mechanisms of rock breakdown by frost action: an experimental approach. Cold Reg Sci Technol 17(3):253–270

Mellor M (1970) Phase composition of pore water in cold rocks. Cold Regions Research and Engineering Laboratory, Hanover

Meng Q, Zhang M, Han L, Pu H, Chen Y (2018) Acoustic emission characteristics of red sandstone specimens under uniaxial cyclic loading and unloading compression. Rock Mech Rock Eng 51(4):969–988

Momeni A, Abdilor Y, Khanlari GR et al (2016) The effect of freeze–thaw cycles on physical and mechanical properties of granitoid hard rocks. B Eng Geol Environ 75(4):1649–1656

Park J, Hyun CU, Park HD (2015) Changes in microstructure and physical properties of rocks caused by artificial freeze–thaw action. B Eng Geol Environ 74(2):555–565

Prick A (1997) Critical degree of saturation as a threshold moisture level in frost weathering of limestones. Permafrost Periglac 8(1):91–99

Sarici DE, Ozdemir E (2018) Determining point load strength loss from porosity, Schmidt hardness, and weight of some sedimentary rocks under freeze–thaw conditions. Environ Earth Sci 77(3):62

Tan XJ, Chen WZ, Yang DS, Dai YH, Wu GJ, Yang JP, Yu HD, Tian HM, Zhao WS (2014) Study on the influence of airflow on the temperature of the surrounding rock in a cold region tunnel and its application to insulation layer design. Appl Therm Eng 67(1–2):320–334

Tan XJ, Chen WZ, Liu HY, Wang LY, Ma W, Chan AHC (2018) A unified model for frost heave pressure in the rock with a penny-shaped fracture during freezing. Cold Reg Sci Technol 153:1–9

Wang P, Xu J, Liu S, Wang H, Liu S (2016) Static and dynamic mechanical properties of sedimentary rock after freeze–thaw or thermal shock weathering. Eng Geol 210:148–157

Wang LP, Li N, Qi JL, Tian YZ, Xu SH (2019) A study on the physical index change and triaxial compression test of intact hard rock subjected to freeze–thaw cycles. Cold Reg Sci Technol 160:39–47

Wang WJ, Yang XL, Huang SB, Yin D, Liu GF (2020) Experimental study on the shear behavior of the bonding interface between sandstone and cement mortar under freeze–thaw. Rock Mech Rock Eng 53:881–907

Watanabe K, Mizoguchi M (2002) Amount of unfrozen water in frozen porous media saturated with solution. Cold Reg Sci Technol 34(2):103–110

Wu T, Liaw HC, Chen YZ (2002) Thermal effect of surface tension on the inward solidification of spheres. Int J Heat Mass Tran 45(10):2055–2065

Xia CC, Lv ZT, Li Q, Huang JH, Bai XY (2018) Transversely isotropic frost heave of saturated rock under unidirectional freezing condition and induced frost heaving force in cold region tunnels. Cold Reg Sci Technol 152:48–58

Yamabe T, Neaupane KM (2001) Determination of some thermomechanical properties of Sirahama sandstone under subzero temperature condition. Int J Rock Mech Min 38(7):1029–1034

Zhang HM, Meng XZ, Yang GS (2020) A study on mechanical properties and damage model of rock subjected to freeze–thaw cycles and confining pressure. Cold Reg Sci Technol 174:103056. https://doi.org/10.1016/j.coldregions.2020.103056

Zhang H, Yuan C, Yang G, Wu L, Peng C, Ye W, Moayedi H (2021) A novel constitutive modelling approach measured under simulated freeze–thaw cycles for the rock failure. Eng Comput 37:779–792. https://doi.org/10.1007/s00366-019-00856-4

Zhao X, Lv X, Wang L, Zhu Y, Dong H, Chen W, Ding Y (2015) Research of concrete residual strains monitoring based on WLI and FBG following exposure to freeze–thaw tests. Cold Reg Sci Technol 116:40–48

Zhou Z, Zhan H, Hu J, Ren C (2019) Characteristics of unloading creep of tuffaceous sandstone in east tianshan tunnel under freeze–thaw cycles. Adv Mater Sci Eng 20:7547564